ORIGINAL RESEARCH ARTICLE

Modeling Static Recrystallization in Al-Mg Alloys

HEINRICH BUKEN and ERNST KOZESCHNIK

In the present work, the influence of Mg on recrystallization kinetics in Al is analyzed by computer simulation. A comprehensive state parameter-based microstructure model is developed, which describes recrystallization in terms of nucleation and growth. The mechanism of solute drag is fully incorporated, thus accounting for the decrease of grain boundary mobility in the presence of impurity atoms. On the basis of the present approach, the solute binding energy between Mg atoms and grain boundaries is assessed and compared to experimentally measured values. Furthermore, the influence of Mg on dislocation production during strain hardening is modeled. The simulations of the composition and temperature-dependent recrystallization kinetics are verified on experimental studies where excellent agreement is achieved. Both simulation and experiment show that increasing Mg content first decelerates and, later on, accelerates recrystallization kinetics.

https://doi.org/10.1007/s11661-020-06100-9

I. INTRODUCTION

THE control of microstructure evolution during processing of Mg-alloyed Al materials is a key factor for determining the final mechanical–technological properties of the material. Mg is a widely used element in Al alloys, especially in the 5xxx and 6xxx series. On the one hand, Mg segregates into grain boundaries and reduces the mobility of the moving boundary by several orders of magnitude in comparison to pure Al.[1] This so-called solute drag effect[2] is caused by solute atoms being dragged along with the moving grain boundary, thus exerting a restraining force against the movement of the grain boundary. As a result, microstructural processes involving the motion of high-angle grain boundaries (HAGB) and low-angle grain boundaries (LAGB) can be severely slowed down by the presence of impurity atoms.[1,3] On the other hand, an increased Mg content promotes a higher strain-hardening rate, which, at identical strain, induces a higher dislocation density.[4,5] As a result, the driving pressure for recrystallization increases, thus accelerating the observed recrystallization kinetics. Koizumi *et al.*[6] have performed recrystallization experiments in Al-Mg alloys, observing that an increase of the Mg content first leads to a deceleration of the rate of recrystallization, followed by an acceleration at further increasing Mg content. These results will form the basis of experimental verification of the present model.

In literature, several approaches are available describing recrystallization phenomena in metallic materials. With particular focus on Al alloys, earlier models[7,8] mostly utilize JMAK-based equations[9] for describing the kinetics of static recrystallization. In these models, several semi-empirical parameters are commonly utilized to adjust the simulated recrystallizing kinetics to experimentally measured recrystallized fractions. Since JMAK-based models do not incorporate explicit mechanism-based descriptions for nucleation and growth of recrystallizing grains, they can only take limited account of basic physical phenomena such as the solute drag effect, precipitate–dislocation interactions in precipitation hardening alloys or the influence of impurities on dislocation generation during strain hardening.

Recently, Zurob *et al.*[10,11] presented a physically based model describing recrystallization with explicit expressions for nucleation and growth. In their work, the nucleation rate for recrystallization is evaluated from microstructural state parameters such as the subgrain size and the dislocation density, which, in combination with growth equations, delivers information on the recrystallized fraction within the deformed microstructure. The solute drag impact is included in the grain boundary mobility within the Cahn approach.[2] When applying the model to Al, however, Zurob *et al.*[10] utilized experimentally determined mobilities taken from literature instead of calculating composition-dependent mobilities based on physical relationships. Furthermore, this work does not take into account that the alloy composition has an important

HEINRICH BUKEN is with the Primetals Technologies Austria GmbH, Turmstrasse 44, 4031 Linz, Austria and also with the Institute of Materials Science and Technology, TU Wien, Getreidemarkt 9, 1060 Vienna, Austria. ERNST KOZESCHNIK is with the Institute of Materials Science and Technology, TU Wien and also with the MatCalc Engineering GmbH, Getreidemarkt 9, 1060 Vienna, Austria. Contact e-mail: ernst.kozeschnik@tuwien.ac.at

Manuscript submitted August 21, 2020; accepted November 6, 2020.

Article published online December 6, 2020

impact on the dislocation evolution during and after deformation. Consequently, no variation in the alloy composition of various Al alloys is elaborated in this work and recrystallization kinetics is evaluated only for a single Mg content of 1 wt pct.

In the present work, a state parameter-based model is developed, in which all relevant microstructural parameters are numerically integrated forward in time. The evolution equations incorporate full composition and temperature dependence for grain boundary mobilities as well as dislocation generation during strain hardening. The calculated grain boundary mobilities are compared to experimentally measured values to illustrate the predictive potential of the present grain boundary mobility approach. In addition, relations, by which the driving pressure for recrystallization is described as a function of the Mg content through a composition-dependent dislocation generation term, are introduced. Furthermore, the previous version of the model, which has been reported in References 12 and 13 is substantially improved in terms of the introduction of the Rayleigh distribution for the rate of supercritical subgrain formation (Section II–A) instead of a sharp limit corresponding to the comparison of the mean and critical subgrain sizes, as well as a dynamic treatment of the subgrain size with growth and shrinkage terms (Section II–B). The predictions of the recrystallization model are finally compared with experimentally measured values from literature. The entire model and input parameters are explained in detail, subsequently.

II. THE RECRYSTALLIZATION MODEL

A. *Nucleation and Growth*

The nucleation rate of newly formed recrystallized grains, $\dot{N}_{\mathrm{rx}}$, is formulated as the product of the number density of potential nucleation sites, N_{pot}, a site saturation factor, B_{nuc}, which accounts for the grain area that is already covered by recrystallized grains and which is, therefore, no longer available for further nucleation, as well as the flux of subgrains reaching supercritical size, $\dot{F}_{\mathrm{sub}}$, as

$$\dot{N}_{\mathrm{rx}} = N_{\mathrm{pot}} B_{\mathrm{nuc}} \dot{F}_{\mathrm{sub}}. \qquad [1]$$

Bailey and Hirsch[14] suggested that the main nucleation mechanism for recrystallization is given by the process of strain-induced boundary migration. This process is initiated when a subgrain being in contact with a high-angle grain boundary (HAGB) exceeds a critical size, r_{crit}, determined by the quotient of the interfacial energy of the HAGB, γ_{HB}, the time,t, and the driving pressure, P_{D}, as determined by the total dislocation density, ρ, with

$$r_{\mathrm{crit}}(t) = \frac{2\gamma_{\mathrm{HB}}}{P_D(t)} = \frac{2\gamma_{\mathrm{HB}}}{0.5\ \mathrm{Gb}\rho(t)}, \qquad [2]$$

with the shear modulus, G, the Burgers vector, b, and r denoting the radius of the subgrain.

The number density of potential nucleation sites can be calculated from the quotient of the specific grain boundary area, a_{av}, per unit volume of material and the area covered by a single supercritical subgrain being located at the high-angle grain boundary. The former is influenced by the degree of deformation of the grain, where the surface area increases with increasing strain. This process is mapped into the simulations using the analysis of Zhu *et al.* [15] who described the evolution of surface area of the grains during deformation in the form of a function, f, depending on the deformation strain, ε. This function represents the ratio of the specific surface area of the deformed grain compared to that of the undeformed grain. The total number of potential nucleation sites, N_{pot}, then reads

$$N_{pot} = \frac{a_{\mathrm{av}}}{\pi r_{\mathrm{crit}}^2} f(\varepsilon). \qquad [3]$$

To calculate the specific grain boundary area of one individual undeformed grain, the grain is assumed to have the shape of a tetrakaidecahedron. The total available grain boundary area of all deformed grains can be formulated in dependence of the mean grain radius, R, the number density of the original grains, N_0, and the surface area of one grain, S_{HAG}, as

$$\begin{aligned} a_{\mathrm{av}} &= 0.5 N_0 S_{\mathrm{HAG}} \\ &= 0.5 \left(\frac{1}{8\sqrt{2}(1.5R)^3} \right) \left(\left(6 + 12\sqrt{3}\right)(1.5R)^2 \right). \end{aligned} \qquad [4]$$

Thereby, the factor 1.5 relates the edge length of the tetrakaidecahedron to its mid-radius.

With the continuous production of new recrystallization nuclei, the deformed grain boundary surface continues to become occupied leading to a continuous decrease of the nucleation rate. To approximate this, the following term is utilized to consider this effect

$$B_{\mathrm{Nuc}} = 1 - \frac{N_{\mathrm{rx}} \pi (r_{\mathrm{crit}})^2}{a_{\mathrm{av}}}. \qquad [5]$$

To describe the distribution of subgrain sizes, a Rayleigh distribution is utilized as experimentally observed by Pantleon and Hansen[16] and also used in the model of Rehman and Zurob.[11] The fraction of subgrains, which are larger than the critical size, can then be expressed as

$$F_{\mathrm{sub}}(t) = \exp\left(-\frac{\pi}{4} \mathrm{X}_{\mathrm{crit}}^2(t) \right), \qquad [6]$$

where $\mathrm{X}_{\mathrm{crit}}$ is the critical subgrain size normalized with respect to the mean subgrain size. The fraction of subgrains, which become supercritical and serve as new stable recrystallization nuclei, is found after differentiation with respect to time as

$$\dot{F}_{\mathrm{sub}} = -\frac{1}{2} \pi F(t) X_{\mathrm{crit}} \dot{X}_{\mathrm{crit}}. \qquad [7]$$

The normalized critical subgrain size and its derivative, $\dot{X}_{\text{crit}}$, are calculated in dependence of the actual mean subgrain size, r_{mean}, and the critical subgrain size, as

$$X_{\text{crit}}(t) = \frac{r_{\text{crit}}(t)}{r_{\text{mean}}(t)} \quad [8]$$

and

$$\dot{X}_{\text{crit}} = \frac{\dot{r}_{\text{crit}}}{r_{\text{mean}}} - \frac{r_{\text{crit}}\dot{r}_{\text{mean}}}{r_{\text{mean}}^2}. \quad [9]$$

Successfully nucleated recrystallized grains grow into the deformed grains by dissipation of the stored deformation energy. This process is modeled by formulating a growth rate, $\dot{R}_{\text{rx}}$, as the product of a driving pressure, P_{D}, (identical to the one in Eq. [2]) and an effective high-angle grain boundary mobility, $M_{\text{eff,HB}}$, from Reference 12 with

$$\dot{R}_{\text{rx}} = M_{\text{eff,HB}} P_{\text{D}} (1 - X_{\text{rx}}). \quad [10]$$

The growth rate is scaled with the recrystallized volume fraction, X_{rx}, in order to account for hard impingement of the recrystallized grains.

Since the driving pressure for nucleation and growth of recrystallized grains is provided by the stored deformation energy, *i.e.,* the dislocation density, this quantity and its evolution as function of temperature, strain rate, and chemical composition of the alloy play a central role in modeling recrystallization kinetics. This is equally true for the growth rate of recrystallized grains, Eq. [10], as well as the nucleation rate as defined in Eqs. [1 and 2]. Consequently, particular emphasis of the present work has been directed into accurate modeling of this microstructural state parameter.

The evolution of the dislocation density is described by means of an extended Kocks–Mecking model[17] considering the processes of dislocation generation as well as dynamic and static recovery. In this context, the approach introduced by Sherstnev *et al.*[18] is closely followed, describing the rate of the total dislocation density as

$$\dot{\rho} = \frac{M\sqrt{\rho}}{\text{Ab}}\dot{\varepsilon} - 2B\frac{d_{\text{ann}}}{b}\rho M\dot{\varepsilon} - 2\text{CD}_{\text{Dis}}\frac{Gb^3}{k_B T}(\rho^2 - \rho_{\text{RS}}^2), \quad [11]$$

with the Taylor factor, M, the critical dislocation annihilation distance, d_{ann}, the substitutional self-diffusion coefficient at dislocations, D_{Dis}, the strain rate, $\dot{\varepsilon}$, and material-dependent coefficients A, B, C. In contrast to the original Sherstnev *et al.* model, where the driving force for static recovery is given by the difference of actual and equilibrium dislocation density, a limiting degree of static recovery is introduced, here, given by the amount of geometrically necessary dislocations, ρ_{RS}, for maintaining the subgrain microstructure. In the Read–Shockley model,[19] the mean subgrain misorientation angle, θ_{mean}, and the mean subgrain size in a periodic network of subgrains define the geometrically necessary dislocation density as

$$\rho_{\text{RS}} = \frac{\tan(\theta_{\text{mean}})}{b r_{\text{mean}}}. \quad [12]$$

Finally, the individual pieces of information about nucleation density and growth rate are combined to calculate the increase of the recrystallized volume fraction as

$$\dot{X}_{\text{rx}} = 27\sqrt{2}\left(R_{\text{rx}}^3 \dot{N}_{\text{rx}} + 3N_{\text{rx}}R_{\text{rx}}^2\dot{R}_{\text{rx}}\right) = \frac{\dot{V}_{\text{rx}}}{V_{\text{tot}}}. \quad [13]$$

In evaluation of the grain volume of all recrystallized grains in the matrix, V_{rx}, it is again assumed that the grain geometry can be approximated by a tetrakaidecahedron. Since the model refers to unit volume of material, the total volume, V_{tot}, is 1 m^3.

A major advantage of the present nucleation model is that it avoids the (extensive) use of fitting parameters in the form of activation energies. Instead, the essential temperature and composition dependencies of the nucleation rate, Eq. [1], are incorporated within the evolution equations for the mean subgrain size, r_{mean}, as well as the composition and temperature-dependent evolution of the critical nucleation radius, r_{crit}, Eq. [2], which in turn is determined by the dislocation density evolution, Eq. [11]. The composition and temperature dependency of the growth rate is also inherently incorporated in the high-angle grain boundary mobility, $M_{\text{eff,HB}}$, as well as the driving pressure, P_{D}. As a result, the present model utilizes only a minimum number of undetermined input parameters with most of the temperature dependence of physical quantities already being determined by the temperature dependence of independently measured quantities, such as the bulk and grain boundary self-diffusion coefficients as well as solute drag binding energies as obtained from the application of the corresponding Cahn model.[2]

B. *Subgrain Evolution*

As emphasized in the previous section, the nucleation rate for recrystallization is substantially determined by the evolution of the mean subgrain size in relation to the critical subgrain size for recrystallization nuclei. In the present approach, the evolution of mean subgrain size is formulated in differential form as superposition of a shrinkage term, $\dot{r}_{\text{S}}^-$, and a growth term, $\dot{r}_{\text{G}}^+$, with

$$\dot{r}_{\text{mean}} = \dot{r}_{\text{S}}^- + \dot{r}_{\text{G}}^+. \quad [14]$$

A convenient parameterization of this general equation can be achieved in analogy to (i) the "principle of similitude," as introduced by Estrin *et al.*[20] and Nes,[21] to describe the impact of dislocation storage on the reduction of the subgrain size and (ii) the driving force—mobility concept, as already used to describe the growth rate of recrystallizing grains, Eq. [10]. Although the former represents a convenient relation between the

mean subgrain size and the average dislocation density in several deformed materials, as analyzed by, e.g., Gil Sevillano *et al.*,[22] it has also been shown that the similitude relation is strictly applicable only to stage II hardening, since, in stages III and beyond, localized slip phenomena (microbanding) and crystal or grain breakup can occur.[23] In the present work, this relation is, therefore, only applied in its differential form as

$$\dot{r}_S^- = \frac{\partial}{\partial t}\left(\frac{A'}{\sqrt{\rho}}\right) = -2A'\left(\frac{r_{\text{mean}}}{A'}\right)^3 \dot{\rho}_{\text{gen}}, \qquad [15]$$

being aware that it reduces to a more or less empirical relation for larger degree of deformation with only limited correspondence to the original principle of similitude. A' is a material-dependent shrinkage coefficient for the effect of dislocation generation and storage on subgrain size evolution and $\dot{\rho}_{\text{gen}}$ is the dislocation generation rate.

In an investigation of the evolution of subgrains during annealing, Sandstrom[3] observed that the rate of subgrain growth is inversely proportional to the current subgrain size. Based on this work, Ørsund and Nes[24] described the growth of subgrains in terms of mobility and driving pressure. Later, Huang and Humphreys[25] experimentally investigated subgrain growth in pure Al and also successfully applied a model that describes the growth rate via mobilities and driving pressures. This approach is adopted, here, for the subgrain growth rate as

$$\dot{r}_G^+ = M_{\text{eff,LB}} \cdot P_{\text{D,SGG}}, \qquad [16]$$

with an effective LAGB mobility, $M_{\text{eff,LB}}$, and the driving pressure for subgrain growth, $P_{\text{D,SGG}}$.

In conventional approaches to subgrain growth, e.g., References 3, 24, 25 only the interface curvature-dependent contribution to the driving pressure is considered. In a recent work, Bréchet *et al.*[26] extend this approach and formulate an additional restraining pressure generated by the intrinsic dislocation density. The integral driving pressure for subgrain growth then reads

$$P_{\text{D,SGG}} = \frac{2\gamma_{\text{LB}}}{r_{\text{mean}}} - \frac{Gb^2}{\sqrt{2\delta r_{\text{mean}}}}\sqrt{\rho_{\text{int}}}, \qquad [17]$$

with the subgrain boundary energy, γ_{LB}, the interaction width of the LAGB, δ, and the internal dislocation density, $\rho_{\text{int}} = \rho - \rho_{\text{RS}}$, describing the statistically distributed dislocations.

The subgrain boundary mobility, Eq. [23] later, incorporates the temperature dependence of the subgrain growth rate as well as the impact of impurity atoms, *i.e.,* the solute drag effect. The parameterization of this quantity is outlined in the following section.

C. *Boundary Mobility*

The grain and subgrain boundary mobilities are most important input parameters determining the recrystallization kinetics. To model the HAGB mobility, the same approach is used, which has recently been successfully applied to recrystallization kinetics simulations in micro-alloyed steel[13] with

$$M_{\text{eff,HB}} = \left(\frac{1}{M_{\text{free,HB}}} + \frac{1}{M_{\text{SD}}}\right)^{-1}, \qquad [18]$$

where $M_{\text{free,HB}}$ is the mobility of the free undisturbed boundary and M_{SD} is the solute drag-affected mobility capturing the influence of impurity atoms. The former can be calculated from the work of Turnbull[27] as

$$M_{\text{free;HB}} = \eta_{\text{free,HB}} \cdot M_{\text{TB}} = \eta_{\text{free,HB}} \cdot \frac{\omega D_{\text{GB}} V_{\text{m}}}{b^2 RT} \qquad [19]$$

with the efficiency factor, $\eta_{\text{free,HB}}$, the grain boundary width, ω, the grain boundary self-diffusion coefficient, D_{GB}, the molar volume, V_{m}, the ideal gas constant, R, and the temperature, T. The diffusion coefficient along grain boundaries has been independently assessed, recently, by Stechauner and Kozeschnik[28] and their values are adopted, here. The efficiency factor for the free mobility is adjusted to the experimental data of[1] and delivers good results for $\eta_{\text{free}} = 0.4$.

The effect of solute drag is accounted for on the basis of the classical Cahn approach,[2] where the solute drag mobility, M_{SD}, is inversely proportional to the concentration of impurity atoms in the grain boundary, C_{GB}, and an inverse mobility, α, as

$$M_{SD} = \frac{1}{\alpha C_{GB}} \qquad [20]$$

and

$$\alpha = \frac{\omega (RT)^2}{E_{\text{B}} D_{\text{CB}} V_{\text{M}}}\left(\sinh\left(\frac{E_{\text{B}}}{RT}\right) - \left(\frac{E_{\text{B}}}{RT}\right)\right), \qquad [21]$$

where E_{B} is the interaction energy between the solute drag-exerting element and the grain boundary. A value of 5 kJ / mol is utilized for this quantity. D_{CB} is the diffusion coefficient across the grain boundary. The concentration of Mg, C_{GB}, is assumed to be identical to the matrix concentration.[11, 13, 29]

If the Mg content in the alloy increases, the grain boundary mobility decreases due to the increasing amount of atoms that must be dragged along with the moving boundary. In the limit of zero Mg, the calculated integral mobility approximates the free mobility since the solute drag mobility approaches infinity. Figure 1 compares the calculated grain boundary mobilities to experimental data, where fair agreement is achieved.

Sandstrom[3] and Winning *et al.*[30] suggest that dislocation climb provides a viable mechanism for subgrain boundary movement. On this basis, Sandstrom[3] formulates a mobility approach, where the subgrain boundary mobility, M_{SS}, is mainly a function of the bulk diffusion coefficient, D_{B}, which is applicable to pure alloys. In the present approach, a temperature-independent linear prefactor, $\eta_{\text{free,LB}}$, is introduced, which determines the value of the effective free boundary mobility as

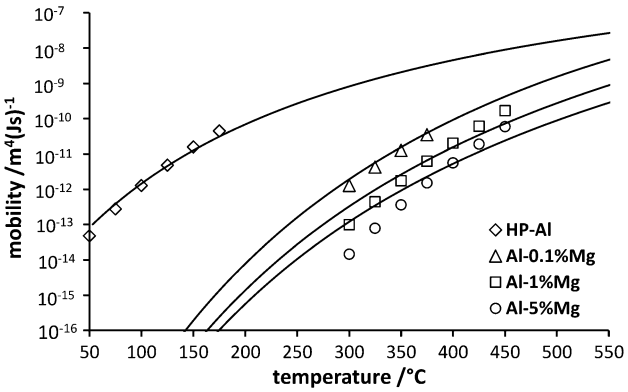

Fig. 1—Calculated (solid lines) and experimental (symbols) grain boundary mobility for Al-5 pctMg, Al-1 pctMg, Al-0,1 Mg pct, and high-purity Al at different temperatures. Experimental data from Huang and Humphreys.[1]

$$M_{\text{free;LB}} = \eta_{\text{free,LB}} \cdot M_{\text{SS}} = \eta_{\text{free,LB}} \cdot \frac{D_{\text{B}} b^2}{k_{\text{B}} T} \qquad [22]$$

with the Boltzmann constant, k_{B}. In their simulations, Rehman and Zurob[11, 31] observe that the growth rate of subgrains is slowed down by dissolved atoms. Therefore, they introduce a model that correlates the rate of subgrain growth with the mean distance of solute atoms. Unfortunately, a separate parameter must be defined for each type of solute and obstacle, which is somehow decoupled from the parameters of the remaining simulation structure.

In contrast to the Rehman and Zurob approach, the influence of solute atoms on subgrain growth is interpreted again as being somehow proportional to the effect of solutes on grain boundary movement as delivered by the Cahn model.[2] Although not directly grounded on a physical basis, a subgrain boundary retardation factor is introduced, which is derived from the ratio of free and solute drag mobilities of the high-angle grain boundaries as

$$M_{\text{eff,LB}} = \left(\frac{M_{\text{eff,HB}}}{M_{\text{free,HB}}} \right) M_{\text{free,LB}}. \qquad [23]$$

The major advantage of this approach is the fact that no additional independent calibration parameters must be introduced for the subgrain boundary mobility. The temperature dependence of the mobility is determined by the model of Sandstrom,[3] whereas the composition dependence of the subgrain boundary mobility is related to that of the high-angle grain boundary.

D. *Verification Experiments*

To verify the simulation, the work of Koizumi *et al.*[6] is analyzed, who experimentally investigate the recrystallization kinetics of five different Al alloys with Mg matrix concentrations, C_{Mg}, of 0.5 wt pct, 1 wt pct, 2 wt pct, 3 wt pct, 4 wt pct, and 5 wt pct. In their analysis, they first cast the alloys and measured a grain size of 300 μm after pre-annealing at 450 °C for 7 hours. Subsequently, cold reduction with a total strain of 0.95 is applied and the specimens are finally tempered at temperatures of 225 °C, 250 °C, 275 °C, and 300 °C. During tempering, the specimens are periodically extracted from a salt bath and analyzed metallographically in order to obtain the recrystallized fraction evolution. Since the aim of the present investigation is to model the influence of temperature and composition (solute drag and dislocation evolution accompanying strain hardening) on recrystallization kinetics, only parameters (temperature and composition) are varied, which are relevant to these effects.

E. *Model Input Parameters*

The bulk and grain boundary diffusion coefficients entering the present model are taken from a recent analysis by Stechauner and Kozeschnik.[28] These values mainly determine the temperature dependence of the free boundary mobilities and the static recovery kinetics of dislocations and subgrain boundaries. For the HAGB energy, a value of 0.65-0.0005·T[K] is assumed, which incorporates the temperature dependence of the shear modulus as reported in Reference 32. The resulting specific HAGB energy spans a range of 0.35 J/m^2–0.4 J/m^2 for the considered testing temperatures from 300°C to 225°C, which is well in line with the grain boundary energy value suggested by Murr.[33] The temperature dependency of these values is adopted in the present work, since the results presented later demonstrate good correspondence with experiments. A similar Ansatz for determining the HAGB energy was used by Zurob *et al.*[34] for the austenite phase of steel.

The dislocation density evolution parameters A, B, C are adjusted to the experimental flow curve measurements of Sherby *et al.*[4] by means of applying the Taylor equation[5] with a dislocation strengthening parameter, α_{Taylor}, of 0.2.[35] In the present simulation approach, the dependency of strain hardening on the Mg content is accounted for by the dislocation generation parameter, A, in dependence of the Mg content, as suggested by Kreyca and Kozeschnik,[36] at room temperature. Thereby, the strain-induced dislocation strengthening contribution to the material, σ_{DS}, is expressed as

$$\sigma_{DS} = \sigma_0 + \alpha_{\text{Taylor}} M G b \sqrt{\rho}, \qquad [24]$$

where $\sigma_0$is the thermal contribution to the yield strength containing basic strength as well as solid solution and grain boundary hardening. To apply the above formula, Eq. [11] is used together with the parameters A, B, C given in Table I. Figure 2 shows the simulated flow curves and dislocation densities for high-purity Al, Al-0.5 pctMg, Al-1 pctMg, Al-1.5 pctMg, and Al-3 pctMg, where excellent agreement is achieved.

III. RESULTS AND DISCUSSION

In this section, the simulation results are compared with the experimental data of Koizumi *et al.*,[6] who carried out recrystallization kinetics measurements on a

Table I. List of Simulation Parameters

Symbol	Designation	Value	Unit	References
D_B	Al bulk diffusion coefficient	1.4×10^{-5} exp(-127200/RT)	m^2/s	28
D_{Dis}	Dislocation pipe diffusion	1.5×10^{-6} exp(-83200/RT)	m^2/s	28
D_{GB}	Grain boundary diffusion	2.0×10^{-5} exp(-60200/RT)	m^2/s	28
D_{CB}	Cross boundary diffusion		m^2/s	11, 13
A, B, C	Strengthening parameters	$-16.6\times\ln(C_{Mg})+44.6;2;4\times10^{-5}$	—	This work, 4
A'	similitude parameter		—	12
E_B	Binding energy	5000	J/mol	This work, 1
$C_{GB,Mg}$	HAGB concentration of Mg	C_{Mg}	mol/mol	11, 13
γ_{HB}	HAGB energy	0.65-0.0005×T [K]	J/m^3	This work
γ_{LB}	LAGB energy		J/m^3	32
ω	Grain boundary width	10^{-9}	m	12, 37
b	Burgers vector	2.86×10^{-10}	m	38
δ	Dislocation interaction width	50	m	This work
G	Shear modulus	29438.4-15.052T[K]	MPa	39
θ_{mean}	Mean misorientation angle	3°	—	13
$\eta_{free,HB}$	HAGB prefactor	0.4	—	1
$\eta_{free,LB}$	LAGB prefactor	1	—	25
α_{Taylor}	Strengthening coefficient	0.2	—	35

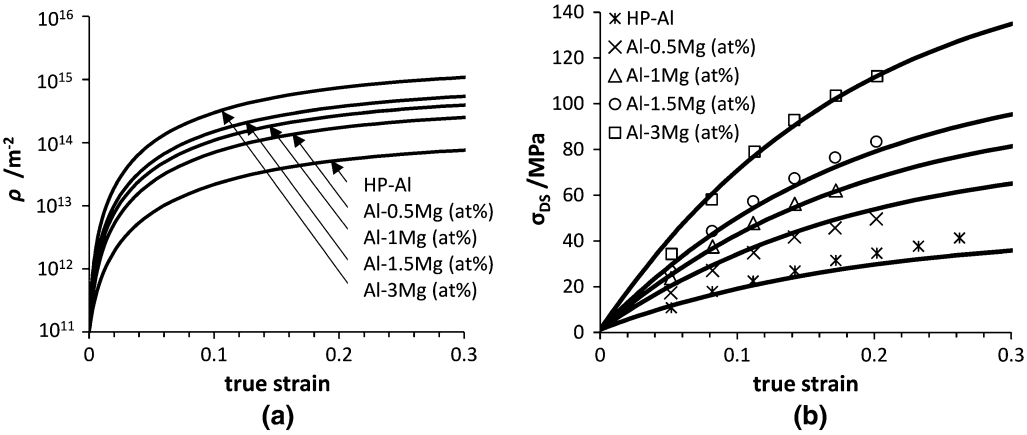

Fig. 2—(*a*) Dislocation generation in dependence of different Mg contents (high-purity Al, Al-0.5 pctMg, Al-1 pctMg, Al-1.5 pctMg, Al-3 pctMg) at 25°C. (*b*) Resulting dislocation strengthening contribution in comparison to experimental data of Ref. [4] at 25 °C.

series of Al-Mg alloys (see Section II–C). In the considered experiments, the recrystallized volume fraction is measured metallographically so that there is more confidence in the measured values than in strength relaxation-based methods, such as double-hit compression tests or hardness measurements.[40] The simulations are carried out with the thermokinetic software tool MatCalc, in which the identical set of input parameters is used (Section II–D) for each simulation (material and temperature variation). The simulation results in comparison to the experiments performed by Koizumi *et al.*[6] are shown in Figure 3.

Koizumi *et al.*[6] observe approximately one order of magnitude difference in recrystallization time for each chemical composition of Al-Mg alloys, when the annealing temperature increases by 25 K. The main reason for this behavior lies in the variation of grain boundary mobility, by which the temperature dependence of the growth rate is determined.

Figure 3 already indicates that the simulations fully reproduce the experimental observation that increasing Mg content first decelerates and then accelerates the rate of recrystallization, see Perryman.[41] A minimum of the recrystallization rate can be found in the Koizumi experiments[6] at a Mg content of approximately 1 wt pct. This behavior can be described by the interplay of two mechanisms triggered by Mg atoms in the Al matrix: On one hand, increasing Mg content decreases the grain boundary mobility due to the solute drag effect exerting a retarding pressure on the boundary during migration.[2] Consequently, this effect acts as a retarding process on recrystallization (Eq. [10]). To quantify this mechanism, Figure 1 displays the simulated boundary mobility for various concentrations of Mg in the matrix (Section II–B) compared to experimental data.

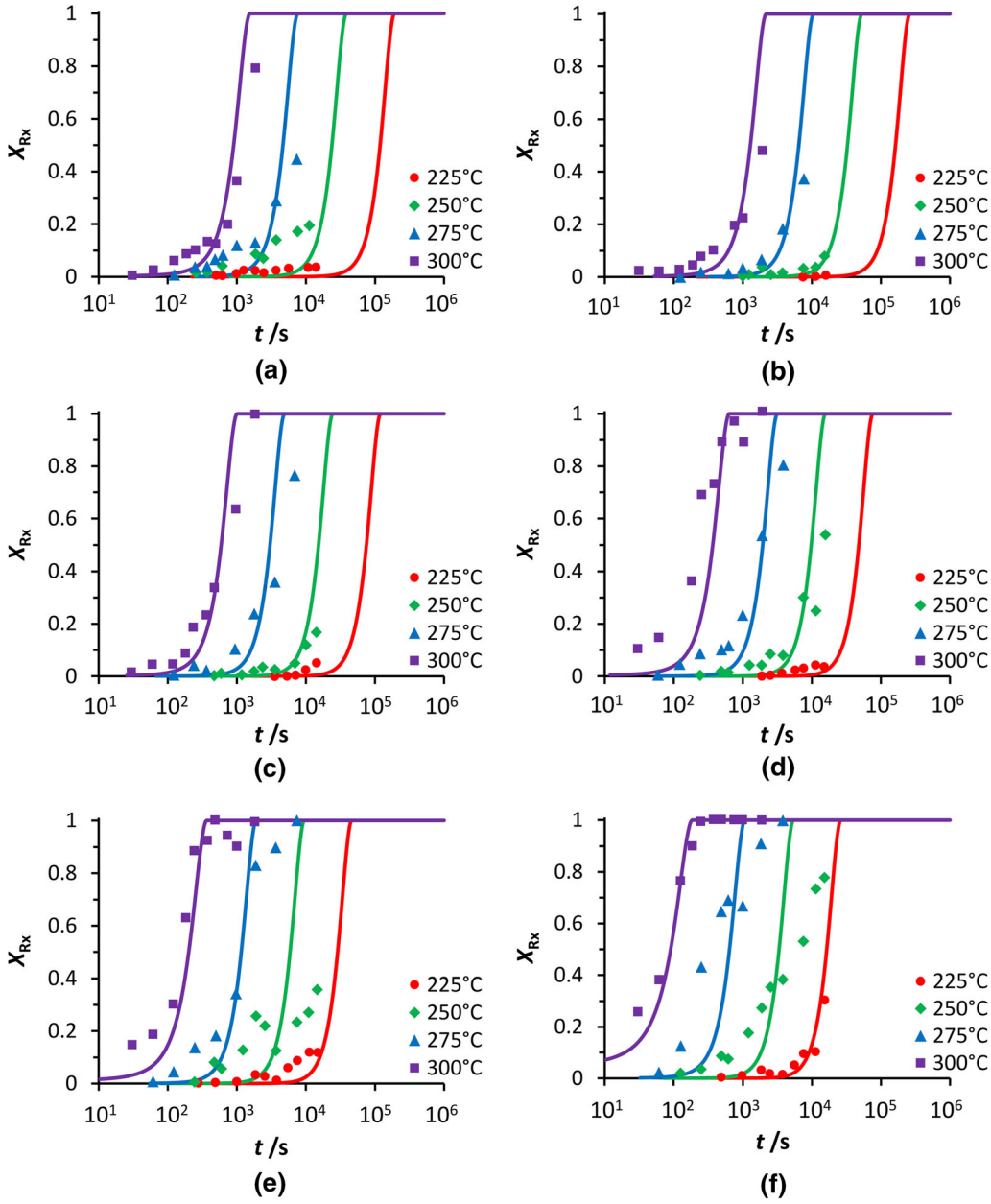

Fig. 3—Calculated recrystallization kinetics at different temperatures for (*a*) Al-0.5 pctMg, (*b*) Al-1 pctMg, (*c*) Al-2 pctMg, (*d*) Al-3 pctMg, (*e*) Al-4 pctMg, and (*f*) Al-5 pctMg.

On the other hand, the dislocation evolution is heavily dependent on the Mg content. In a recent contribution, Muzyk *et al.*[42] point out that Mg has a strong influence on the stacking fault energy in Al alloys. Kocks and Mecking[17] suggest that the strain-hardening potential in materials should scale with the stacking fault energy. Thornton *et al.*[43] describe that the change in stacking fault energy influences the cross-slip mechanism of dislocations at high temperatures and, thus, leads to a lower rate of dynamic recovery. In their recent analysis, Kreyca and Kozeschnik[36] show that both, the rate of dislocation generation and that of dislocation annihilation due to dynamic recovery, are influenced by the Mg content.

The two mechanisms referenced above, solute drag and dislocation density evolution, severely interact in the present simulation. As a consequence, the observed recrystallization kinetics can be likewise accelerated and decelerated, depending on the Mg content. Figure 4 summarizes the influence of the Mg content on recrystallization kinetics. In image 4a), the simulated recrystallized volume fractions at 275°C are compared, showing that the recrystallization kinetics are faster in Al-0.5 pctMg compared to Al-1 pctMg. A further increase in Mg always leads to an increase of the recrystallization kinetics. Diagram 4b) shows the simulated (markers) and measured (line) 50 pct recrystallization temperatures. Excellent agreement between the

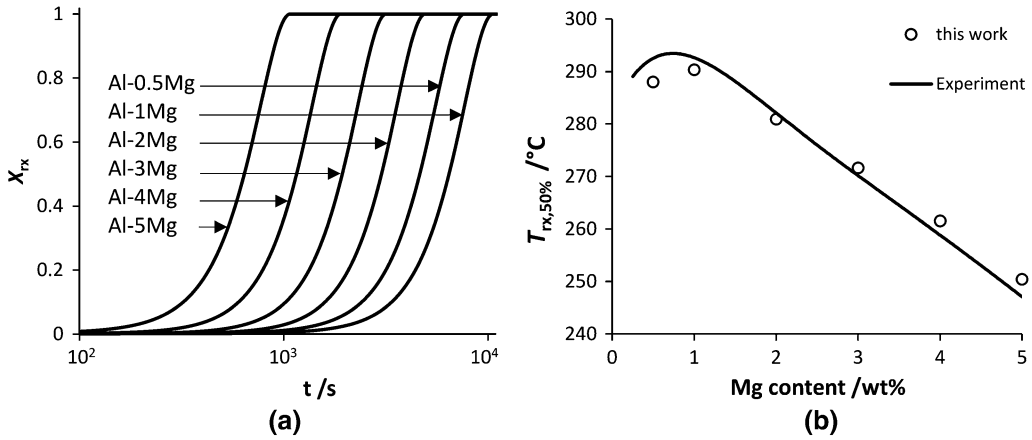

Fig. 4—(*a*) Simulated recrystallization kinetics at 275°C for all considered alloys. (*b*) Simulated 50 pct recrystallization temperature (markers) and experimental data from Ref. [6] (line).

experimental observations and the simulations based on the present model is observed.

IV. SUMMARY

In the present work, a comprehensive state parameter-based model for static recrystallization in terms of nucleation and growth of recrystallizing grains is proposed. Both the HAGB mobilities and the dislocation densities are evolved on the basis of physical evolution expressions and they are individually analyzed and compared to independent experiments. On one hand, the Mg content-dependent dislocation density evolution promotes recrystallization with increasing alloy content due to increased dislocation production. On the other hand, the solute drag effect retards recrystallization due to an increasingly retarding effect on boundary mobility. The mutual interplay of these effects is observed in both the simulation and the experiment.

FUNDING

Open access funding provided by TU Wien (TUW).

OPEN ACCESS

REFERENCES

1. Y Huang and FJ Humphreys: *Mater. Chem. Phys.*, 2012, vol. 132, pp. 166–74.
2. JW Cahn: *Acta Metall.*, 1962, vol. 10, pp. 789–98.
3. R Sandstrom: *Acta Metall.*, 1977, vol. 25, pp. 905–11.
4. OD Sherby, RA Anderson, and JE Dorn: *JOM*, 1951, vol. 3, pp. 643–52.
5. G. I. Taylor: *Proc. R. Soc. A Math. Phys. Eng. Sci.*, 1934, vol. 145, pp. 362–87.
6. M Koizumi, S Kohara, and H Inagaki: *Zeitschrift Für Met.*, 2000, vol. 91, pp. 460–67.
7. FJ Humphreys: *Acta Mater.*, 1997, vol. 45, pp. 4231–40.
8. T Furu, K Marthinsen, and E Nes: *Mater. Sci. Technol.*, 1990, vol. 6, pp. 1093–1102.
9. Melvin Avrami: *J. Chem. Phys.*, 1940, vol. 8, pp. 212–24.
10. HS Zurob, Y Bréchet, and J Dunlop: *Acta Mater.*, 2006, vol. 54, pp. 3983–90.
11. K. Rehman and H. S. Zurob: *Metall. Mater. Trans. A Phys. Metall. Mater. Sci.*, 2013, vol. 44, pp. 1862–71.
12. H Buken, P Sherstnev, and E Kozeschnik: *Model. Simul. Mater. Sci. Eng.*, 2016, vol. 24, p. 35006.
13. H. Buken and E. Kozeschnik: *Metall. Mater. Trans. A Phys. Metall. Mater. Sci.*, 2017, vol. 48, pp. 2812–18.
14. J. E. Bailey and P. B. Hirsch: *Proc. R. Soc. A Math. Phys. Eng. Sci.*, 1962, vol. 267, pp. 11–30.
15. Q Zhu, CM Sellars, and HKDH Bhadeshia: *Mater. Sci. Technol.*, 2007, vol. 23, pp. 757–66.
16. W Pantleon and N Hansen: *Acta Mater.*, 2001, vol. 49, pp. 1479–93.
17. UF Kocks and H Mecking: *Prog. Mater. Sci.*, 2003, vol. 48, pp. 171–273.
18. P. Sherstnev, P. Lang, and E. Kozeschnik: in *Eur. Congr. Comput. Methods Appl. Sci. Eng. (ECCOMAS 2012), 10.-14.9.2012*, J. Eberhardsteiner et.al., ed., Vienna, Austria, 2012, pp. 1–8.
19. WT Read and W Shockley: *Phys. Rev.*, 1950, vol. 78, p. 275.
20. Y. Estrin, L.S. Tóth, a. Molinari, and Y. Bréchet: *Acta Mater.*, 1998, vol. 46, pp. 5509–22.
21. E Nes: *Prog. Mater. Sci.*, 1997, vol. 41, pp. 129–93.
22. J. Gil Sevillano, P. Van Houtte, and E. Aernoudt: *Prog. Mater. Sci.*, 1980, vol. 25, pp. 69–412.
23. K Marthinsen and E Nes: *Mater. Sci. Technol.*, 2001, vol. 17, pp. 376–88.
24. R Ørsund and E Nes: *Scr. Metall.*, 1989, vol. 23, pp. 1187–92.
25. Y Huang and FJ Humphreys: *Acta Mater.*, 2000, vol. 48, pp. 2017–30.

26. YJM Bréchet, HS Zurob, and CR Hutchinson: *Int. J. Mater. Res.*, 2009, vol. 100, pp. 1446–48.
27. D Turnbull: *Trans. Am. Inst. Min. Met. Eng.*, 1951, vol. 191, pp. 661–65.
28. G Stechauner and E Kozeschnik: *Calphad Comput. Coupling Phase Diagrams Thermochem.*, 2014, vol. 47, pp. 92–99.
29. H. Buken, P. Sherstnev, and E. Kozeschnik: in *Mater. Sci. Forum*, 2017, pp. 2463–67.
30. M Winning, AD Rollett, G Gottstein, DJ Srolovitz, A Lim, and LS Shvindlerman: *Philos. Mag.*, 2010, vol. 90, pp. 3107–28.
31. K Rehman and HS Zurob: *Mater. Sci. Forum*, 2013, vol. 753, pp. 417–22.
32. H. Buken and E. Kozeschnik: in *IOP Conf. Ser. Mater. Sci. Eng.*, 2016, p. 012023.
33. L.E. Murr: *Interfacial Phenomena in Metal and Alloys*, Addison-Wesley Publishing Company, Reading, 1977.
34. HS Zurob, CR Hutchinson, Y Brechet, and G Purdy: *Acta Mater.*, 2002, vol. 50, pp. 3075–92.
35. ME Kassner: *Acta Mater.*, 2004, vol. 52, pp. 1–9.
36. J Kreyca and E Kozeschnik: *Int. J. Plast.*, 2018, vol. 103, pp. 67–80.
37. T. Zhou, R. J. O'Malley, and H. S. Zurob: *Metall. Mater. Trans. A Phys. Metall. Mater. Sci.*, 2010, vol. 41, pp. 2112–20.
38. H. Frost and M. Ashby: *Deformation Mechanism Maps: The Plasticity and Creep of Metals and Ceramics*, 1982.
39. EI Galindo-Nava, J Sietsma, and PEJ Rivera-Díaz-Del-Castillo: *Acta Mater.*, 2012, vol. 60, pp. 2615–24.
40. HS Zurob, CR Hutchinson, Y Brechet, and GR Purdy: *Mater. Sci. Eng. A*, 2004, vol. 382, pp. 64–81.
41. E.C.W. Perryman: *Trans. AIME*, 1955, pp. 369–78.
42. M Muzyk, Z Pakiela, and KJ Kurzydlowski: *Scr. Mater.*, 2011, vol. 64, pp. 916–18.
43. PR Thornton, TE Mitchell, and PB Hirsch: *Philos. Mag.*, 1962, vol. 7, pp. 1349–69.